Electronic Supplementary Material (ESI) for Physical Chemistry Chemical Physics.

Supporting Information for

Distinctive Phase Separation Dynamics of Polymer Blends: Roles of Janus Nanoparticles

Qing Li, Liquan Wang, Jiaping Lin*, Liangshun Zhang*

Shanghai Key Laboratory of Advanced Polymeric Materials, State Key Laboratory of Bioreactor Engineering, Key Laboratory for Ultrafine Materials of Ministry of Education, School of Materials Science and Engineering, East China University of Science and Technology, Shanghai 200237, China

* Tel: +86-21-64253370; E-mail: jlin@ecust.edu.cn (J. Lin), lq_wang@ecust.edu.cn (L. Wang)

Contents

1. Dissipative Particle Dynamics

In this work, a mesoscopic method entitled dissipative particle dynamics (DPD) was adopted to perform the simulations. In this method, each bead represents a lump of atomic or molecular matters. Its movement is governed by the following equations of motion:[S1]

$$\frac{d\mathrm{r}_i}{dt} = \mathrm{v}_i, \; m\frac{d\mathrm{v}_i}{dt} = \mathrm{f}_i$$

where t is the time; m is the mass; $\mathbf{r}_i$ and $\mathbf{v}_i$ are the position and velocity of the ith bead, respectively; and $\mathbf{f}_i$ is the force applied on it. The $\mathbf{f}_i$ consists of four parts, *i.e.*, a conservative force $\mathbf{F}_{ij}^{\mathrm{C}}$, a dissipative force $\mathbf{F}_{ij}^{\mathrm{D}}$, a random force $\mathbf{F}_{ij}^{\mathrm{R}}$, and a spring bond force $\mathbf{F}_{ij}^{\mathrm{S}}$:

$$\mathbf{f}_i = \sum_{j \neq i} (\mathbf{F}_{ij}^{\mathrm{C}} + \mathbf{F}_{ij}^{\mathrm{D}} + \mathbf{F}_{ij}^{\mathrm{R}} + \mathbf{F}_{ij}^{\mathrm{S}})$$

The conservative force $\mathbf{F}_{ij}^{\mathrm{C}}$ is a soft repulsive interaction given by

$$\mathbf{F}_{ij}^{\mathrm{C}} = a_{ij}\sqrt{\omega^{\mathrm{C}}(r_{ij})}\hat{\mathbf{r}}_{ij}$$

where a_{ij} is the interaction parameter; $\hat{\mathbf{r}}_{ij}$ is a unit vector pointing from the jth bead to the ith bead; r_{ij} is the distance between them; and $\omega^{\mathrm{C}}(r_{ij})$ is a weight function equal to $(1 - r_{ij}/r_{\mathrm{c}})^2$ at $r_{ij} < r_{\mathrm{c}}$ and equal to 0 at $r_{ij} \geq r_{\mathrm{c}}$, with r_{c} being the cut-off distance. The dissipative force $\mathbf{F}_{ij}^{\mathrm{D}}$ is dependent on the relative velocities of the ith and jth beads:

$$\mathbf{F}_{ij}^{\mathrm{D}} = -\gamma\omega^{\mathrm{D}}(r_{ij})(\hat{\mathbf{r}}_{ij} \cdot \mathbf{v}_{ij})\hat{\mathbf{r}}_{ij}$$

where γ is the friction coefficient; $\omega^{D}(r_{ij})$ is a weighting function; and $\mathbf{v}_{ij} = \mathbf{v}_i - \mathbf{v}_j$. The random force is defined by

$$\mathbf{F}_{ij}^{R} = \mu\omega^{R}(r_{ij})\Gamma_{ij}\Delta t^{-1/2}\hat{\mathbf{r}}_{ij}$$

where μ is the noise amplitude, $\omega^{R}(r_{ij})$ is a weighting function, Δt is the time step, and Γ_{ij} is a randomly fluctuating variable obeying the Gaussian statistics:

$$\langle \Gamma_{ij}(t) \rangle = 0, \langle \Gamma_{ij}(t)\Gamma_{kl}(t) \rangle = (\delta_{ik}\delta_{jl} + \delta_{il}\delta_{jk})\delta(t - t')$$

The $\omega^{D}(r_{ij})$ and $\omega^{R}(r_{ij})$ are related by $\omega^{D}(r_{ij}) = [\omega^{R}(r_{ij})]^2 = \omega^{C}(r_{ij})$, and the values of γ and μ are coupled by $\mu^2 = 2\gamma k_B T\Delta t$, where k_B and T are the Boltzmann constant and the temperature, respectively. By this means, the equilibrium states corresponding to the canonical (NVT) ensemble can be achieved.[S1] In addition, a spring force $\mathbf{F}_{ij}^{S}$ was used to connect adjacent beads in homopolymer chains and JP grafting blocks:

$$\mathbf{F}_{ij}^{S} = C(1 - r_{ij}/r_{eq})\hat{\mathbf{r}}_{ij}$$

with C and r_{eq} being the spring constant and the equilibrium distance, respectively. In the present work, the magnitudes of γ and μ are set to be 4.5 and 3.0, respectively. The magnitude of the spring constant is chosen to be $C = 30$, and the equilibrium distance is set to be $r_{eq} = 0.86r_c$.

2. Influence of the Volume Fraction of Janus Nanoparticles

Fig. S1a shows the impact of the volume fraction c_{JP} of Janus particles on the time evolution of the first moment q_1 of the structure factor $S(q)$ for JP-compatibilized P_A/P_B blends. It can be seen that the slope of the $q_1(t)$ curve decreases as the c_{JP} increases. As stated in the Models and Methods section, the value of q_1 is inversely related to the average size of polymer domains at the late stage. Therefore, the decrease in the slope of $q_1(t)$ indicates that the late-stage domain growth has been effectively retarded. Fig. S1b displays the growth exponent n (obtained from the slope of the q_1 profile) as a function of the particle loading. The decrease of n with increasing c_{JP} once again demonstrates the retarded phase separation dynamics of JP-compatibilized blends at the late stage.

Furthermore, we found that the values of $q_1(t)$ at very late times (*e.g.*, $t = 10^4\tau$; see Fig. S1b) is linearly dependent on the c_{JP} at $c_{JP} > 0.1$. This can be attributed to the interfacial activity of Janus particles.[S2-S4] Hore and Laradji studied the influence of surface-active nanoparticles on the domain growth dynamics of homopolymer blends.[S2] They argued that the effective interfacial tension σ_{eff} is time-dependent at the late stage, as the nanoparticles adsorb onto the interfaces and reduce the unfavorable interactions between dislike components. In this case, the average domain size $R(t)$ is given by the following equation:

$$R(t) = \frac{\alpha R_{NP}}{c_{NP}} - \left(\frac{\alpha R_{NP}}{c_{NP}} - R_0\right)e^{-t/\tau_s} \tag{S8}$$

where $R(t) \sim 1/q_1$; α is a coefficient depending on the geometry of polymer domains; R_{NP} and c_{NP} are the radius and volume fraction of nanoparticles, respectively; R_0 is the initial value of the domain size; and the time scale τ_s is given by $\tau_s = (\alpha\eta R_{JP})/\gamma_{AB}c_{JP}$, with η the viscosity of homopolymers and γ_{AB} the interfacial tension between the P_A and P_B domains when the nanoparticles are absent. Eq. S8 implies that the $q_1(t)$ is proportional to the volume fraction of nanoparticles at $t >> \tau_s$. As shown in Fig. S1b, this is the

case for JP-compatibilized blends, which corroborates the capability of Janus particles to reduce the effective interfacial tension during the late stage. (The linear law stated above is not satisfied at $c_{JP} < 0.1$, because the particle loading is too low.)

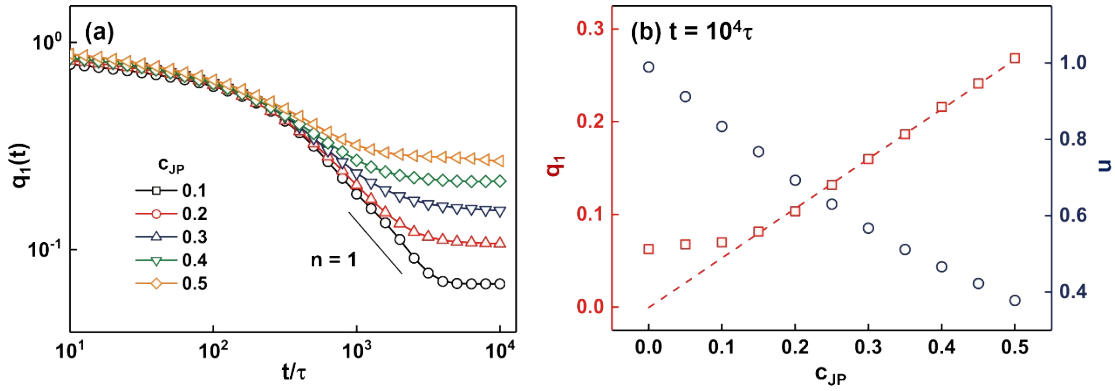

Figure S1. (a) Time evolution of the first moment q_1 of the structure factor at various c_{JP} values. Red solid line denotes the growth exponent n of compatibilizer-free blends. (b) Dependence of the q_1 (red squares) and n (blue circles) on the particle loading c_{JP} at the very late time $t = 10^4\tau$. Red dashed line denotes the linear fitting of the q_1 values.

3. Comparison of Different Additives

Fig. S2 shows the structure factor $S(q)$ at the very early times for pure P_A/P_B blends (panel a) and blends with various additives, including the triblock copolymers (TCPs; panel b), the HP–I particles (panel c), the HP–II particles (panel d), and the Janus particles (panel e). It can be found that only the blend with the Janus particles incorporated exhibits remarkable $S(q)$ peaks, which demonstrates that only the Janus particles can facilitate the development of the dominant composition fluctuation.

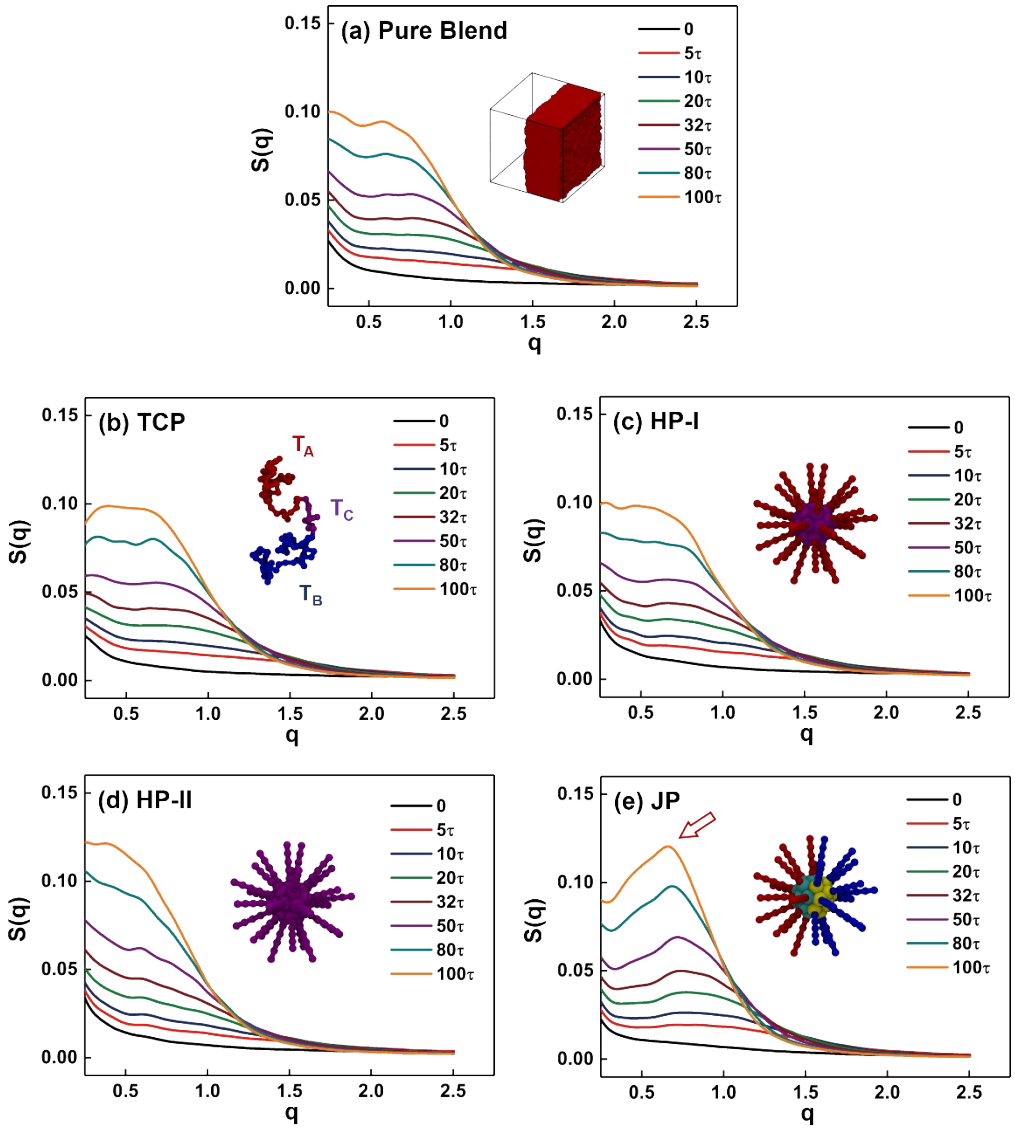

Figure S2. Structure factor $S(q)$ at the very early times for (a) pure P_A/P_B blends and P_A/P_B blends with various additives, including (b) triblock copolymers (TCPs), (c) HP–I particles, (d) HP–II particles, and (e) Janus particles (JPs). Volume fraction of additives are fixed to be 0.2. Inset in panel (a) shows the equilibrium morphology of the pure blend, with the P_A domain colored in red and the P_B domain omitted for clarity. Insets in other panels show the coarse-grained models of corresponding additives. Red arrow in panel (e) indicates the peak in the $S(q)$ profile at $t = 100\tau$.

4. Size of Homopolymer-Rich Regions near Janus Particles

Fig. S3 shows the method to evaluate the size $L(t)$ of homopolymer-rich (enrichment) regions in the vicinity of Janus particles. We first calculate the ensemble-averaged composition $\varphi(\mathbf{r})$ (see the Models and Methods section) at positions along the major axis of Janus particles (the straight line passing through the mass centers of the J_A and J_B hemispheres), and then obtain the position where the $\varphi(\mathbf{r})$ is equal to a setting value φ_s (= 0.9), which is indicated by hollow arrows in Fig. S3a and b.

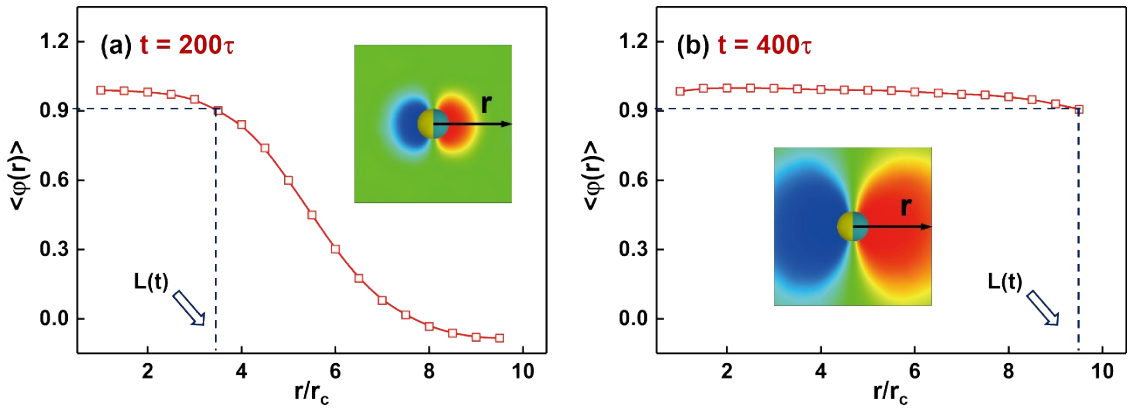

Figure S3. Ensemble-averaged composition $\varphi(r)$ along the r-arrows at (a) $t = 200\tau$ and (b) $t = 400\tau$, for the blends with the particle loading $c_{JP} = 0.2$. Inset in each panel shows the ensemble-averaged distribution of the $\varphi(\mathbf{r})$ around the Janus particles.

5. Time Evolution of Enrichment Region Size

Fig. S4 shows the time-dependent size $L(t)$ of enrichment regions near Janus particles at increasing particle loadings (c_{JP}). Before the critical time t_c (see Fig. 2c for the definition of t_c), the influence of the particle loading on the growth dynamics of $L(t)$ is not remarkable. The curves of $L(t)$ diverges at the critical time t_c, and the blends with larger particle loadings exhibit smaller $L(t)$ values. We attribute the decrease of $L(t)$ with increasing c_{JP} at $t > t_c$ to the interfacial activity of Janus particles.

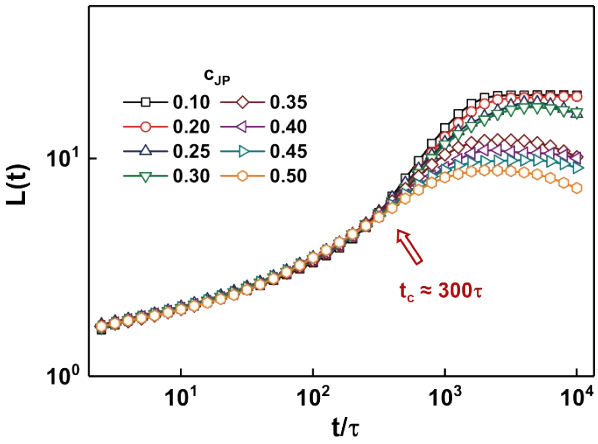

Figure S4. Size $L(t)$ of the **A**-rich regions at various c_{JP} values. Red arrow indicates the critical time t_c corresponding to the crossover of $S(q^*)$ curves (see Fig. 2c).

6. Enrichment Region around the HP–I Nanoparticles

In order to gain a clear insight into the development of enrichment regions, we studied the formation of P_A-rich regions around the counterparts of JPs whose grafting blocks are composed of the **A** component (*i.e.*, HP-I particles). Fig. S5 shows the number densities of respective components in the vicinity of HP–I particles at various times. One can clearly identify the formation of **A**-rich regions around the particles. However, the enrichment regions shown in Fig. S5 lack the microphase-separated nature of those around Janus particles, which indicates that the anisotropic structure of JPs is the prerequisite of the development of microphase-separated enrichment regions.

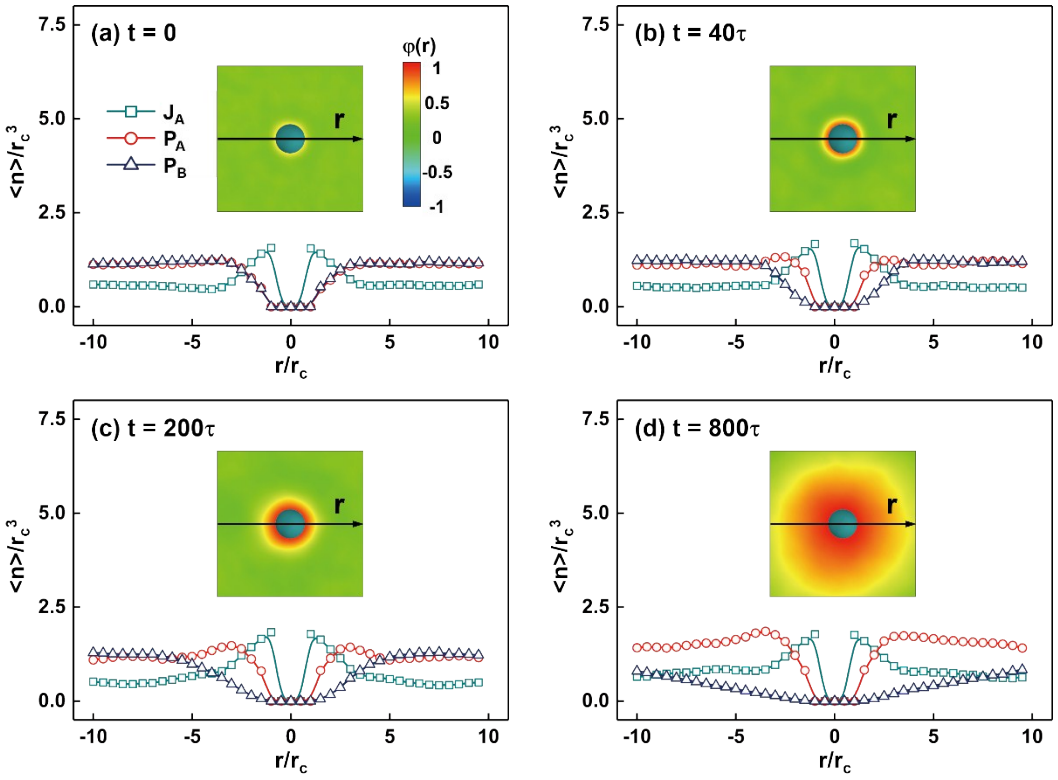

Figure S5. Ensemble-averaged density n of respective components along the r-arrows at (a) $t = 0$, (b) $t = 40\tau$, (c) $t = 200\tau$, and (d) $t = 800\tau$ for blends with the HP–I particles incorporated. Volume fraction c_{HP} of HP–I particles is 0.2.

7. Mean Square Displacement

Fig. S6 shows the mean square displacement (MSD) of the mass centers of Janus particles (panel a) and homopolymers (panel b) as a function of time t at various c_{JP} values. It can be viewed that the <MSD> of JP mass centers is much smaller than that of the mass centers of homopolymers at the early times ($t < t_c$), which confirms that the phase separation at early times is governed by the movement of homopolymers.

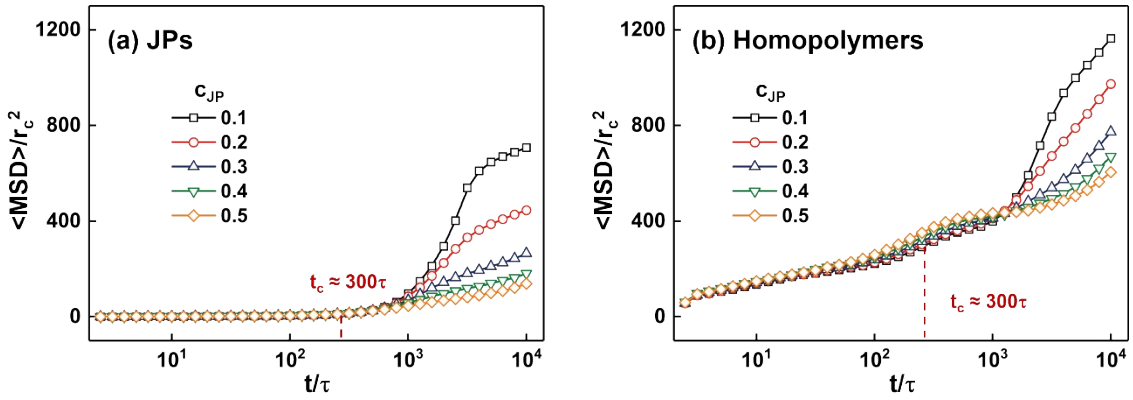

Figure S6. Mean square displacement (MSD) of the mass centers of (a) Janus particles and (b) P_A/P_B homopolymers at various times t for blends with various particle loadings (c_{JP}).

8. Mechanism behind the JP-induced Local Microphase Separation

In the present work, we have demonstrated that the distinctive phase separation dynamics of JP-compatibilized blends is closely related to the formation of microphase-separated homopolymer-rich regions around Janus particles. The mechanism underlying such JP-induced local microphase separation can be comprehended by comparing it with the surface-directed spinodal decomposition (SDSD).[S5-S9] For a mixture confined between two selective planar surfaces, one can observe the formation of an enrichment layer followed by a depletion layer in the vicinity of each surface, which acts as the anchoring center for the dominant SD wave that propagates from the surface into the bulk.[S5] In our work, the two surface parts of JPs can also act as the anchoring centers for the dominant SD wave. Nevertheless, most of the SDSD studies so far were concerned with planar surfaces, whereas the surfaces of JPs are highly curved, which leads to the hemispherical shape of **A**/**B**-rich regions as shown in Fig. 3. Such a difference indicates the critical influence of surface shape on the development of enrichment regions

The unique promoting effect of Janus particles at the early stage can be further elaborated on an intuitive level by comparing the formation of **A**/**B**-rich regions with the development and growth of nuclei in a nuclear-growth (NG)-type phase separation system, for which the accidently generated particles of the minority phase (nuclei) can act as pinning centers for the growth of droplets.[S10] Similarly, the J_A and J_B hemispheres can also act as the pinning centers for the growth of phase-separated **A**/**B**-rich regions (see Fig. 3). However, there exists an important difference between the growth mechanisms of the NG droplets and the JP-induced enrichment regions. In the case of NG-type phase separation, the growth of droplets proceeds *via* the steady diffusional fluxes from smaller droplets to nearby larger ones, which leads to the growth of the latter in expense of the former (evaporation-condensation mechanism).[S11-S13] In contrast, such selective domain growth is absent for blends with JPs incorporated, as the growth of enrichment

regions is driven by the diffusional fluxes of homopolymers from the bulk toward the enrichment regions.

9. Phase Separation Dynamics of Compatibilizer-free Blends

Fig. S7 shows the morphological evolution of a representative compatibilizer-free (pure) blend. After the start of the phase separation, the homopolymers P_A and P_B gradually segregate into bi-continuous networks at the early times (see the first row), which further grow into completely separated layers at the late times (the second row). These observations are in good agreement with theoretical predictions and experiments.[S14-S15]

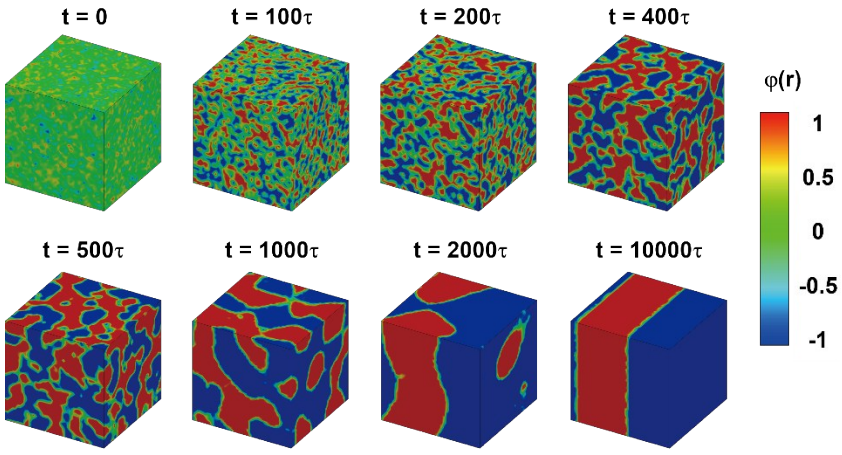

Figure S7. Position-dependent composition $\varphi(\mathbf{r})$ at various times t for a representative pure blend.

We further characterized the phase separation dynamics *via* the structure factor $S(q)$, whose value at a certain scattering vector q is proportional to the amplitude of the SD wave of wavelength $1/q$. As shown in Fig. S8a, the values of $S(q)$ are initially very small at all q values, indicating that the P_A and P_B are uniformly mixed. As the time elapses, a distinctive peak in the $S(q)$ profile develops, which indicates the appearance of the domain SD wave. As the phase separation progresses (panels b and c), the coarsening of phase-separated structures leads to the shift of the peak position toward smaller q values, and the narrowing of the interfaces results in the rapid growth of the $S(q)$ peak intensity. At the very late times

(panel c), both the position and intensity of the $S(q)$ peak become time-invariant, which confirms that the equilibrium state has been achieved.

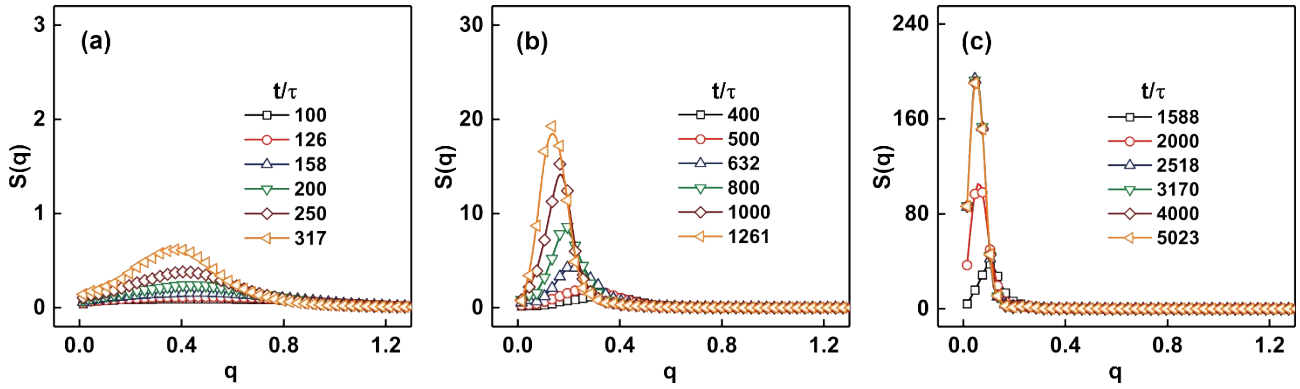

Figure S8. Structure factor $S(q)$ at various times for pure P_A/P_B blends.

Moreover, we plotted in Fig. S9a and b the scaled structure factor $q_1^3S(q)$ at the early and late times, respectively. The profiles of $q_1^3S(q)$ collapse onto a single master curve at the late times (see panel b), which indicates that the phase separation of pure P_A/P_B blends proceeds *via* the self-similar mechanism at the late stage (see Eq. 4 of the Models and Methods section).

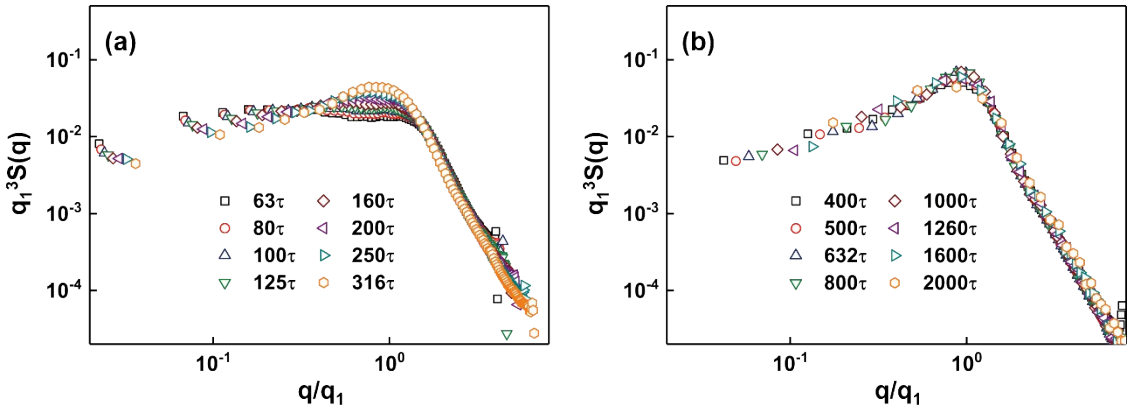

Figure S9. Scaled structure factor $q_1^3S(q)$ for pure P_A/P_B blends at various times.

Lastly, we calculated the first moment q_1 of the structure factor at various times, and displayed the results in Fig. S10. It can be viewed that the time evolution of q_1 obeys the power law noted in Eq. 5, with value of the growth exponent n comparable to the theoretically predicted value (= 1). The results shown in Fig. S9-10 are in good agreement with conventional SD theories[S16-S17], which supports the validity of the simulation method.

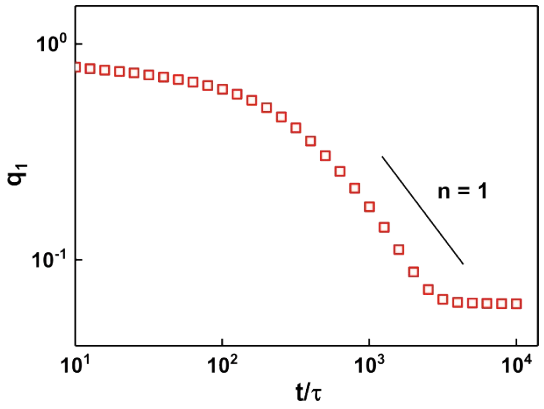

Figure S10. Time evolution of the first moment q_1 of the structure factor $S(q)$ for pure P_A/P_B blends. Black line denotes the theoretically predicted value of the growth exponent n.

10. Influence of the Lengths of JP Grafting Chains

The phase separation dynamics presented in the main text were all concerned with JPs with $N_{graft} = 5$. However, one may question whether the lengths of J_A/J_B chains also influence the phase separation of JP-compatibilized blends. Considering this, we studied the phase separation of P_A/P_B blends at various N_{graft} values ($N_{graft} = 5$, 10, 15, 20), and Fig. S11a-b show the morphological evolution during phase separation for two representative systems (*i.e.*, those compatibilized by JPs with $N_{graft} = 5$ and $N_{graft} = 20$). We found that the blend at $N_{graft} = 20$ shows larger average size of P_A/P_B domains because the number of JPs in a system decreases with increasing N_{graft} values. (Note that $c_{JP} = 0.3$ for both systems). The phase separation dynamics were further characterized in terms of the structure factor $S(q)$, as is shown in Fig. S11c-d. The system compatibilized by JPs with longer grafting chains (panel d) shows stronger early-time $S(q)$ peaks (indicated by the blue arrows), which implies that the promoting effects of JPs at the early stage is enhanced as the N_{graft} increases. This can be attributed to the favorable interactions between the P_A/P_B homopolymers and their liked JP grafting chains, which leads to the formation of **A**/**B**-rich regions near JP surfaces (see Fig. 3 of the main text).

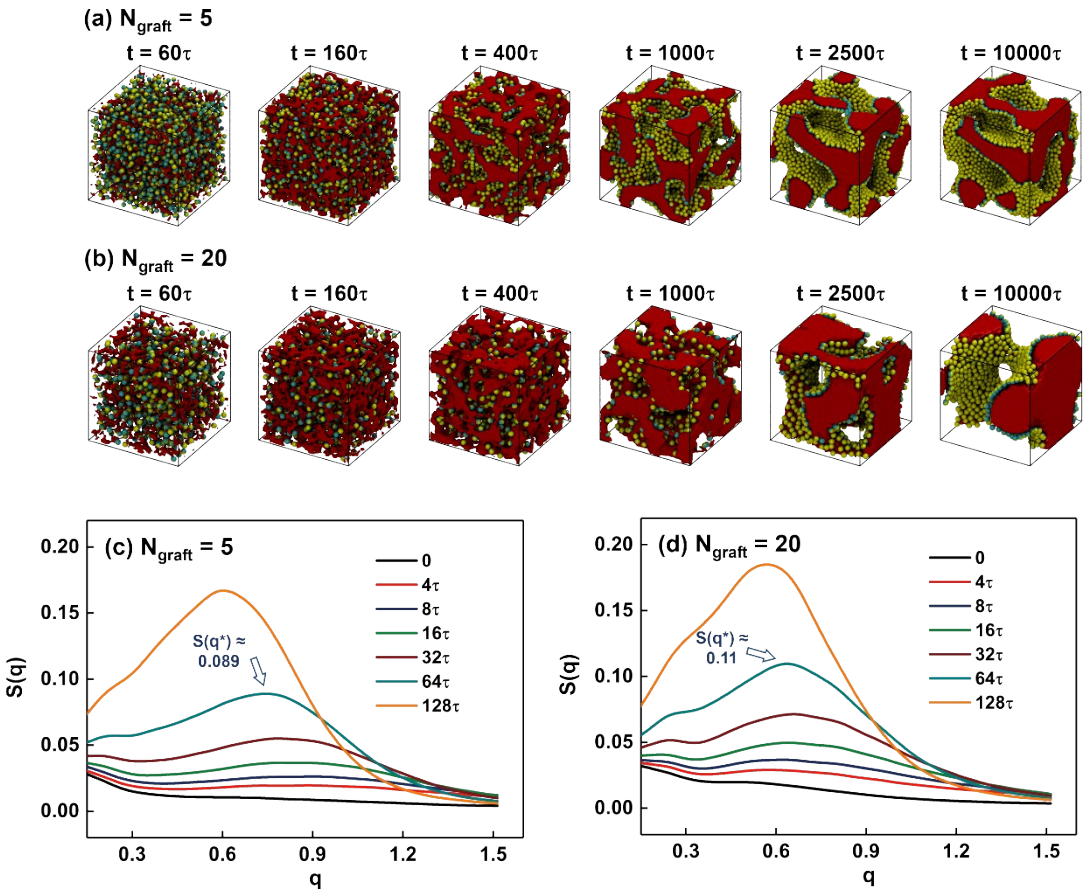

Figure S11. (a-b) Morphologies of JP-compatibilized blends at various times for blends compatibilized by JPs with (a) N_{graft} = 5 and (b) N_{graft} = 20. (c-d) Evolution of the structure factor $S(q)$ at the early stage for JPs with (c) N_{graft} = 5 and (d) N_{graft} = 20. Peak intensities at $t = 64\tau$ are indicated by blue arrows.

11. Discussion on the Models of the JP and the Homopolymers

As stated in the Methods and Models section, the **A**, **B** and **C** systems considered in this work are very similar. This means that the P_A and P_B homopolymers have the same size, and that the **A**-**A**, **B**-**B** and **C**-**C** interactions are identical as is the case for the **A**-**B**, **A**-**C** and **B**-**C** interaction. In addition, the hetero-beads interactions are stronger than the homo-bead interactions. Therefore, one may question (1) whether such a high symmetry is realistic and (2) what would happen if the sizes of the homopolymers were different, the homo-bead interactions were different, the hetero-bead interactions were different, and the hetero-bead interactions were weaker than the homo-bead interactions. Below are our arguments.

First, we wish to emphasize that the blending system studied here is an *ideal* system based the characteristics of *realistic* systems,[S15, S18] and the treatment of high symmetry has its advantage in focusing the studies on special target by excluding various other influence factors. In fact, such a treatment is usually used in theoretical and simulation studies (see ref.[S19], for example). Moreover, the present study is devoted to elaborate the mechanism governing the phase separation dynamics of JP-compatibilized blends *in general*, and we expect that the ideal system studied here can capture the essential characteristics of phase separation systems in the presence of JP-based compatibilizers.

Second, changing either the size of the P_A/P_B homopolymers or the interactions could, for example, influence the phase separation rate. However, the *general feature* of phase separation dynamics is not affected; that is, the Janus nanoparticles promote the decomposition of dislike polymers in the early stage of spinodal decomposition but retard it during the late stage. Following are the possible influences and our arguments.

Sizes of the Homopolymer Chains It is well known that the phase behavior of a polymer blend can be influenced by the sizes of constituent polymers. For example, at the early stage of SD, the unfavorable

interactions between dislike polymers lead to the formation of phase-segregated domains, with the diffusion of the P_A and P_B polymers acting as the dominant transport process. On the other hand, the diffusion rate of a homopolymer closely depends on its size, as the homopolymer of the larger size usually shows slower diffusional movement. Therefore, the homopolymer with the smaller size would first form well-defined domains followed by the other homopolymer if the sizes of them were different. Note that changing the sizes of the P_A and P_B polymers does not affect the general feature of JP-based compatibilizers (*i.e.*, promoting phase separation at the early times but retarding it at the late times).

Interactions of the Hetero-beads In the present model, the J_A block of JPs and the P_A polymer are both composed of the component **A**, whereas the J_B block and the P_B polymer are both composed of the component **B**. Meanwhile, the J_C core of JPs are wrapped by the J_A and J_B blocks, and cannot directly interact with the P_A/P_B polymers (see Fig. 1a-c of the manuscript). This means that the phase separation dynamics of JP-compatibilized blends is dominantly governed by the interaction energy between the **A** and **B** components (manifested by the a_{AB}), while the effects of the a_{AC} and a_{BC} can be neglected. We expect that the a_{AB} value mainly influences the degree and rate of phase separation, as in the pure blends of two homopolymers. As the a_{AB} value increases, the homopolymer blends can undergo a phase separation from disorder phase, and the phase separation can be stronger. (Note that the general feature of the phase separation system studied here is not influenced by such effects.)

Interactions of the Homo-beads Such a case is not suited for study in DPD simulations. This is because the interaction parameters a_{ii} between homo-beads is determined by the number density ρ of beads ($a_{ii} = 75k_BT/\rho$, with k_B the Boltzmann constant and T the temperature), and are hence set to be identical in the DPD method.[S1] In addition, the hetero-bead interactions are always stronger than the homo-bead interactions in the DPD method. In an actual system, the hetero-bead interactions can be weaker than the

homo-bead interactions only when there are some specific interactions such as hydrogen bonds between hetero-beads (beyond the scope of the present study). Our arguments are consistent with most of the existing DPD works (see ref.[20] for example).

12. Orientation of JPs in Blending Systems

As stated in the main text, the JPs can act as "seeds" for the formation of phase boundaries separating the two immiscible homopolymers (see Fig. 3 and Fig. 4). In order to characterize the effect of this process on the orientation of JPs, we calculated the orientation order parameter S_i for JPs, which is given by

$$S_i = (\sum_{j=1}^{N_n} \mathbf{u}_i \cdot \mathbf{u}_j)/N_n$$

where $\mathbf{u}_i$ is the direction of the i-th JP (defined by the unit vector pointed from the mass center of the J_B hemisphere to the mass center of the J_A hemisphere), and N_n is the number of neighboring JPs of the i-th JP. Here, the *neighboring JP* refers to particles whose distance from the i-th JP is smaller than a critical value (= $2.5r_c$ in this work). It can be learned from Eq. S9 that the value of S_i is comparable with 0 if the i-th JP and its neighbors are randomly oriented. In contrast, the value of S_i is comparable with 1.0 if the directions of these particles are parallel with one another.

Fig. S12 shows the distribution ρ_S of the S_i at various times (c_{JP} = 0.4). At the very early stage (Fig. S12a), we found that $<S_i> \approx 0$, which suggests that the JPs are randomly oriented. As the phase separation proceeds, the position of the ρ_S peak gradually moves toward the larger S_i values (Fig. S12b-d), suggesting that the JPs tend to adopt parallel orientations at the late stage of phase separation (see the insets of Fig. S12). Specifically, the value of $<S_i>$ rapidly increases from ~0.42 at $t = 400\tau$ (Fig. S12b) to ~0.79 at $t = 1000\tau$ (Fig. S12c), which suggests that the JPs can form orderly-oriented structures at the phase boundaries formed at this time interval. Moreover, we plotted in Fig. S13 the dependence of the $<S_i>$ on the time at increasing c_{JP} values. A rapid increase in the value of $<S_i>$ from ~0 to ~1.0 at $10^2\tau \le t \le 10^3\tau$ can be viewed for all systems, indicating that the "face-ordering" shown in Fig. S12 is ubiquitous in JP-compatibilized

blends.

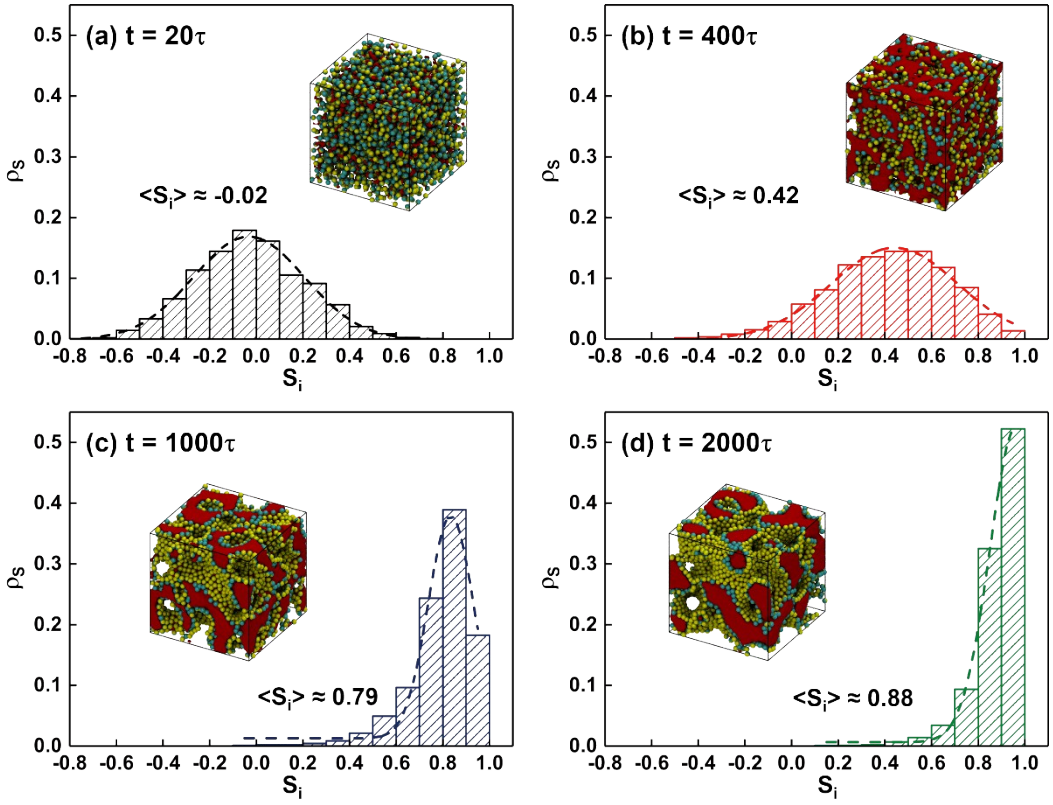

Figure S12. Distribution ρ_S of the orientation ordering parameter S_i for JPs at various times of (a) $t = 20\tau$; (b) $t = 400\tau$, (c) $t = 1000\tau$ and (d) $t = 2000\tau$. $c_{JP} = 0.4$. Inset in each panel shows the morphology of the blend at the corresponding time. Values of the ensemble average of S_i are also indicated.

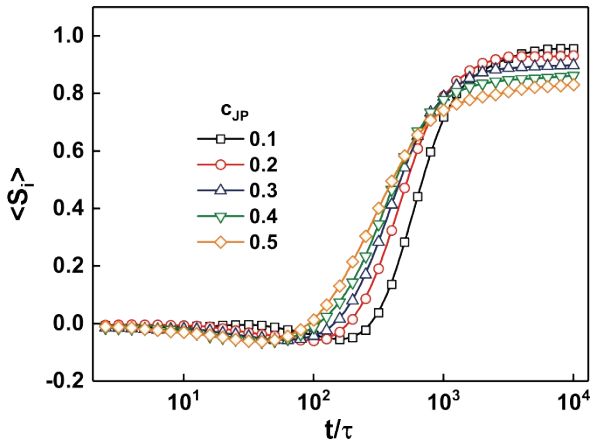

Figure S13. Ensemble average of the order parameter S_i at various times for blends with increasing particle loadings.

References

S1. Groot, R. D.; Warren, P. B. Dissipative Particle Dynamics: Bridging the Gap between Atomistic and Mesoscopic Simulation. *J. Chem. Phys.* **1997,** *107*, 4423-4435.

S2. Hore, M. J. A.; Laradji, M. Microphase Separation Induced by Interfacial Segregation of Isotropic, Spherical Nanoparticles. *J. Chem. Phys.* **2007,** *126*, 244903-244911.

S3. Huang, M.; Li, Z.; Guo, H. The Effect of Janus Nanospheres on the Phase Separation of Immiscible Polymer Blends *via* Dissipative Particle Dynamics Simulations. *Soft Matter* **2012,** *8*, 6834-6845.

S4. Huang, M.; Guo, H. The Intriguing Ordering and Compatibilizing Performance of Janus Nanoparticles with Various Shapes and Different Dividing Surface Designs in Immiscible Polymer Blends. *Soft Matter* **2013,** *9*, 7356-7368.

S5. Puri, S.; Binder, K. Surface-directed Spinodal Decomposition: Phenomenology and Numerical Results. *Phys. Rev. A* **1992,** *46*, R4487-R4489.

S6. Puri, S.; Binder, K. Surface Effects on Spinodal Decomposition in Binary Mixtures and the Interplay with Wetting Phenomena. *Phys. Rev. E* **1994,** *49*, 5359-5377.

S7. Yan, L.-T.; Xie, X.-M. Numerical Simulation of Surface Effects on Spinodal Decomposition in Polymer Binary Mixture: Quench Depth Dependence. *Macromolecules* **2006,** *39*, 2388-2397.

S8. Michels, J. J.; Moons, E. Simulation of Surface-Directed Phase Separation in a Solution-Processed Polymer/PCBM Blend. *Macromolecules* **2013,** *46*, 8693-8701.

S9. Albert, v. B.; Tomasz, Z.; Vsevolod, K.; Jasper, M.; Rene, J.; Martijn, K.; Gerwin, G. Surface Directed Phase Separation of Semiconductor Ferroelectric Polymer Blends and their Use in Non-Volatile Memories. *Adv. Func. Mater.* **2015,** *25*, 278-286.

S10. Ougizawa, T.; Inoue, T., Morphology of Polymer Blends. In *Polymer Blends Handbook*, Utracki, L.

A.; Wilkie, C. A., Eds. Springer Netherlands: Dordrecht, 2014; pp 875-918.

S11. Wagner, C. Theorie der Alterung von Niederschlägen durch Umlösen (Ostwald-Reifung). *Z. Electrochem.* **1961,** *65*, 581-591.

S12. Lifshitz, I. M.; Slyozov, V. V. The Kinetics of Precipitation from Supersaturated Solid Solutions. *J. Phys. Chem. Solids* **1961,** *19*, 35-50.

S13. Shimizu, R.; Tanaka, H. A Novel Coarsening Mechanism of Droplets in Immiscible Fluid Mixtures. *Nat. Commun.* **2015,** *6*, 7407.

S14. Cahn, J. W. Phase Separation by Spinodal Decomposition in Isotropic Systems. *J. Chem. Phys.* **1965,** *42*, 93-99.

S15. Snyder, H. L.; Meakin, P. Details of Phase Separation Processes in Polymer Blends. *J. Polym. Sci. Polym. Symp.* **1985,** *73*, 217-239.

S16. Furukawa, H. A Dynamic Scaling Assumption for Phase Separation. *Adv. Chem. Phys.* **1985,** *34*, 703-750.

S17. Siggia, E. D. Late Stages of Spinodal Decomposition in Binary Mixtures. *Phys. Rev. A* **1979,** *20*, 595-605.

S18. Walther, A; Matussek, K and A. H. E. Müller. Engineering Nanostructured Polymer Blends with Controlled Nanoparticle Location using Janus Particles. *ACS Nano*, **2008**, *2*, 1167-1178.

S19. Jo, W. H.; Kim, S. H. Monte Carlo Simulation of the Phase Separation Dynamics of Polymer Blends in the Presence of Block Copolymers. 1. Effect of the Interaction Energy and Chain Length of the Block Copolymers. *Macromolecules* **1996**, *29*, 7204-7211

S20. Wang, Z; Wang, H; Cheng, M; Li, C; Faller, R; Sun, S; Hu, S. Controllable Multigeometry Nanoparticles *via* Cooperative Assembly of Amphiphilic Diblock Copolymer Blends with Asymmetric

Architectures. *ACS Nano* **2018**, *12*, 1413-1419